# Supporting information

## Lotus-Root-Fiber Inspired Stretchable and Self-Healing Ionic Thermoelectric Gels with Carbon Nanotubes for Enhanced High-Temperature Performance

Jiawei Chen[#,a], Guimei Li [#,a], Wenjun He[a], Chunxia Xie[b], Lan Yang[a], Luoting Wu[a], Manqi Chen[a], Cheng-Gong Han[a,*], Wei Wang[a,*], Li Niu[a,b,*]

a. Center for Advanced Analytical Science, Guangzhou Key Laboratory of Sensing Materials and Devices, Guangdong Engineering Technology Research Center for Photoelectric Sensing Materials and Devices, Key Laboratory of Optoelectronic Materials and Sensors in Guangdong Provincial Universities, School of Chemistry and Chemical Engineering, Guangzhou University, Guangzhou 510006, P. R. China.

b. School of Chemical Engineering and Technology, Sun Yat-Sen University, Zhuhai 519000, P. R. China.

# These authors contributed equally to this work.

*Corresponding Email: hancg@gzhu.edu.cn (Cheng-Gong Han); wangw@gzhu.edu.cn (Wei Wang); lniu@gzhu.edu.cn (Li Niu)

**Content of file**

**Supporting Notes**

**Note S1. Ionic conductivity of i-TE gels**

Electrochemical impedance spectroscopy (EIS) was an effective technique to obtain the ionic conductivity. Graphite paper was used as the electrodes. The internal resistance ($R$) of i-TE gel was derived from the intercept on the real axis in Nyquist plots from EIS measurements. The ionic conductivity ($\sigma_i$), was calculated using the equation $\sigma_i = \frac{l}{RS}$, where $l$ and $S$ represent the gel thickness (0.2 cm) and electrode area (1.0×1.0 $cm^2$), respectively. $R$ values showed a decreased trend as $FeCN^{4-/3-}$ concentration, mass fraction of MWCNTs, and temperature increased, corresponding to the increased ionic conductivity (Figure S10).

**Note S2. Dynamic rheological analysis of i-TE gels**

Temperature-sweep rheological measurement ($\omega$ = 1 Hz, $\gamma$ = 1%, 293-353 K) was performed for the i-TE gel G-0.1M $FeCN^{4-/3-}$-6 wt.%MWCNTs using a rotational rheometer (Rheometer, Shanghai Bosin). In Figure S14, the storage modulus $G'$ maintained the high value (> 4000 Pa) and exceeded the loss modulus $G''$ in the temperature range of 293-303 K, indicating a typical elastic gel state. $G'$ showed a monotonic decrease with a sharp drop near 308 K, and rapidly reached to a low level (< 100 Pa) close to $G''$ above 310 K. This behavior indicated a thermal dissociation of the three-dimensional network and a transition to a sol state dominated by viscous flow. It was noteworthy that the sol-to-gel transition was typically accompanied by a crossover of $G'$ and $G''$ for the chemically crosslinked or strongly physically crosslinked gels, marking an abrupt transition from a viscous fluid ($G' < G''$) to an elastic gel ($G' > G''$). However, in this work, $G'$ for the i-TE gel, as a thermo-reversible physical gel, continuously decayed from a high value while $G''$ remained relatively low and changed mildly, resulting in no strict intersection between them. Nevertheless, the dramatic drop of $G'$ (2-3 times drop) and the evolution of the relative relationship between $G'$ and $G''$ could be confirmed the occurrence of the gel-to-sol transition[1,2].

**Note S3. Thermal performance of i-TE gels**

The melting point and thermal conductivity were critical for assessing the thermal performance of i-TE gels. In differential scanning calorimetry (DSC), the melting points of 309 K and 312 K was observed for G- $FeCN^{4-/3-}$ and G-0.1 M $FeCN^{4-/3-}$-6 wt.% MWCNTs, respectively (Figure S12). It indicated that the improved thermal tolerance was achieved as MWCNTs were introduced. The thermal conductivity ($\kappa$) was calculated using the equation $\kappa = D\rho C_p$, where $D$, $\rho$, and $C_p$ represent the thermal diffusivity, density, and specific heat capacity, respectively. Here, the thermal diffusivity of i-TE gels was measured using a Laser Flash Apparatus (LFA457, NETZSCH). The density of i-TE gel was determined via the mass/volume method. The specific heat capacity of gelatin was employed for caculation for simplicity[3].

The thermal diffusivity of the i-TE gel G-0.1 M $FeCN^{4-/3-}$-6 wt.% MWCNTs increased from 0.12 to 0.16 $mm^2\ s^{-1}$, which was higher than the increase from 0.12 to 0.13 $mm^2\ s^{-1}$ observed for G-0.1 M $FeCN^{4-/3-}$ in the temperature range of 298-323 K (Figure S15(a)). The thermal conductivity increased as rising temperature (Figure S15(b)). At 298 and 323 K, the thermal conductivity of the i-TE gel G-0.1 M $FeCN^{4-/3-}$-6 wt.% MWCNTs was 0.28 and 0.37 $W\ m^{-1}\ K^{-1}$, higher than values of 0.27 and 0.29 $W\ m^{-1}\ K^{-1}$ for G-0.1 M $FeCN^{4-/3-}$, respectively. The MWCNTs in the gel system could enhance the thermal stability of the i-TE gel via the interaction with gelatin molecules and ions. The lower thermal conductivity of G-0.1 M $FeCN^{4-/3-}$-6 wt.% MWCNTs could effectively suppress heat dissipation between the hot and cold electrodes, maintaining a more stable $\Delta T$ during the operation to obtain the stable voltage output (with an ionic thermopower of 11 $mV \cdot K^{-1}$).

**Note S4. $S_{tg}$ ($FeCN^{4-/3-}$) of gels**

For the redox couple containing gel system, a relationship was demonstrated as $S_{tg}$ ($FeCN^{4-/3-}$) = $-\alpha_R = -\Delta S/nF$, where $\alpha_R$, $\Delta S$, $n$, and $F$ represent the temperature coefficient of the electrode, the entropy changes of the redox reaction, the number of electrons transferred, and the Faraday constant, respectively. An isothermal three-electrode system was employed to measure the temperature coefficient $\alpha_R$. This system included a platinum working electrode (WE), a saturated calomel electrode (SCE) as the

reference electrode (RE), and a counter electrode (CE) (Figure S16). The value of $\alpha_R$ was determined from the slope of the open-circuit $V_{oc}$ vs. SCE with dependence of temperature, based on the equation $\alpha_R = dE/dT$. The temperature coefficient $\alpha_R$ ($FeCN^{4-/3-}$) was calculated as the sum of the slope of $V_{oc}$ vs. SCE dependent on temperature and $\alpha_R$ (SCE) (-0.01 mV $K^{-1}$), with the latter measured using a non-isothermal system[4].

The slope of $V_{oc}$ vs. SCE with dependence of temperature for G-0.1 M $FeCN^{4-/3-}$-*y* MWCNTs was -1.55, -1.59, -1.62, and -1.69 mV $K^{-1}$, corresponding to $S_{tg}$ ($FeCN^{4-/3-}$) of 1.56, 1.60, 1.63, and 1.70 mV $K^{-1}$ at *y* = 0 wt.%, 2 wt.%, 4 wt.%, and 6 wt.%, respectively (Figure S17).

**Note S5. Diffusion coefficient of redox couple**

Cyclic Voltammetry (CV) was employed to investigate the electrochemical reactions occurring at the electrode/electrolyte interface and measure the diffusion coefficient (*D*) of the redox couple. An ultramicroelectrode method was employed to obtain the diffusion coefficient. The Pt ultramicroelectrode with a diameter of 20 μm was served as the working electrode. The Pt wire with a diameter of 0.5 mm was used as the counter electrode, and a saturated calomel electrode (SCE) was functioned as the reference electrode. The CV scan was 0.2 mV $s^{-1}$. The diffusion coefficient *D* was calculated using the equation $i_{ss} = 4nFDCr_0$, where $i_{ss}$ represents the limiting current in a steady state, *n* is the number of electrons transferred in the redox reaction, *F* is the Faraday constant, *C* is the concentration of the redox species, and $r_0$ is the radius of the ultramicroelectrode[5]. As shown in Figure S18, the limiting current $i_{ss}$ varied as MWCNTs were sequentially added to the i-TE gels. The diffusion coefficients *D* ($FeCN^{4-/3-}$) were $1.81\times10^{-10}$, $1.53\times10^{-10}$, $1.37\times10^{-10}$ and $0.75\times10^{-10}$ $m^2$ $s^{-1}$ for G-0.1 M $FeCN^{4-/3-}$-*y* MWCNTs composites (*y* = 0 wt.%, 2 wt.%, 4 wt.%, 6 wt.%) at 293 K, respectively. The corresponding diffusion coefficient *D* ($FeCN^{4-/3-}$) of G-0.1 M $FeCN^{4-/3-}$-6 wt.% MWCNTs at 303 and 313 K was $1.04\times10^{-10}$ and $1.45\times10^{-10}$ $m^2$ $s^{-1}$, respectively.

**Supporting Figures**

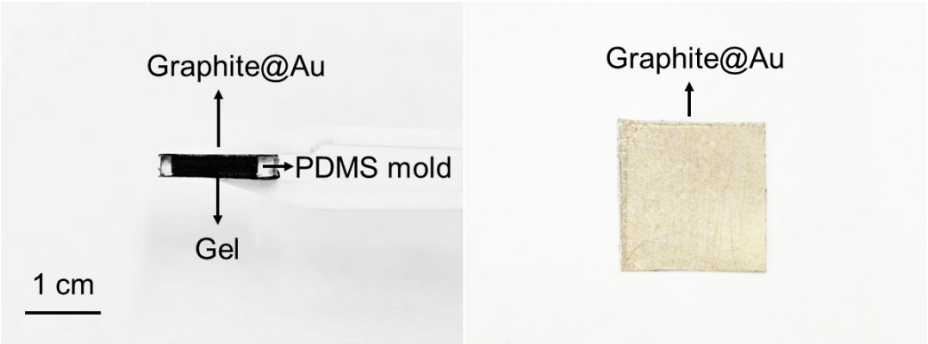


**Figure S1.** Image of i-TE gel thermocell with G-*x* $FeCN^{4-/3-}$-*y* MWCNTs.

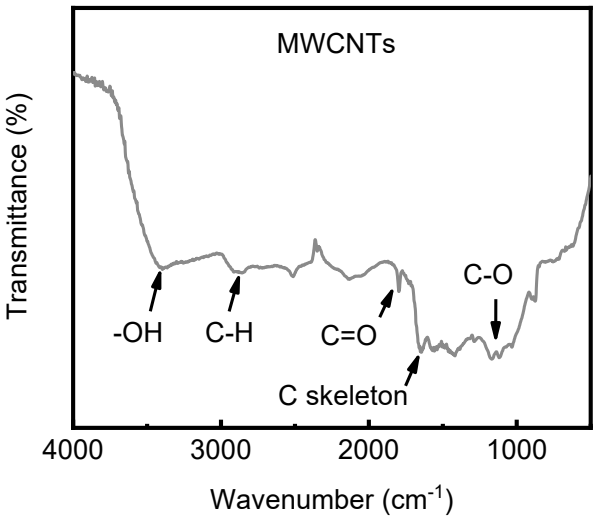


**Figure S2**. Fourier transform infrared spectroscopy (FTIR) of MWCNTs.

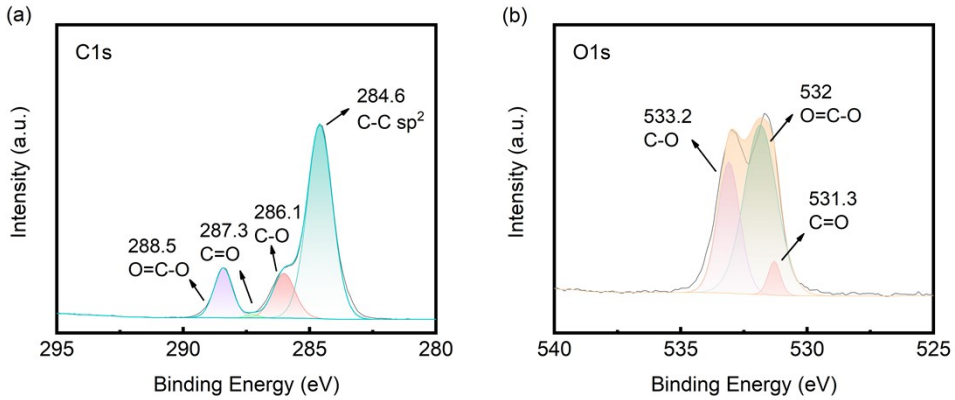


**Figure S3**. High-resolution XPS spectra of MWCNTs. (a) C1s, (b) O1s. The content of carboxyl carbon (O=C-O) was calculated to be 8.76 at% through semi-quantitative analysis of the XPS C1s spectrum using peak area integration.

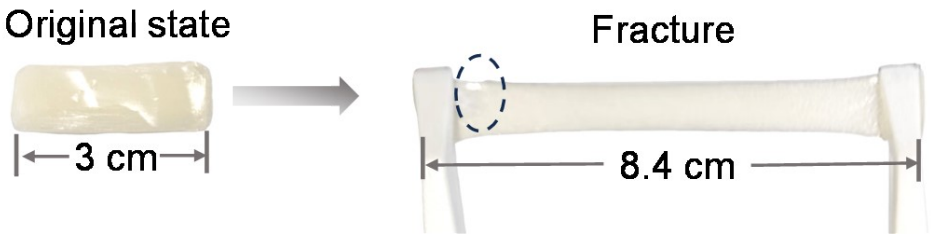


**Figure S4.** Stretchable image of pure gelatin.

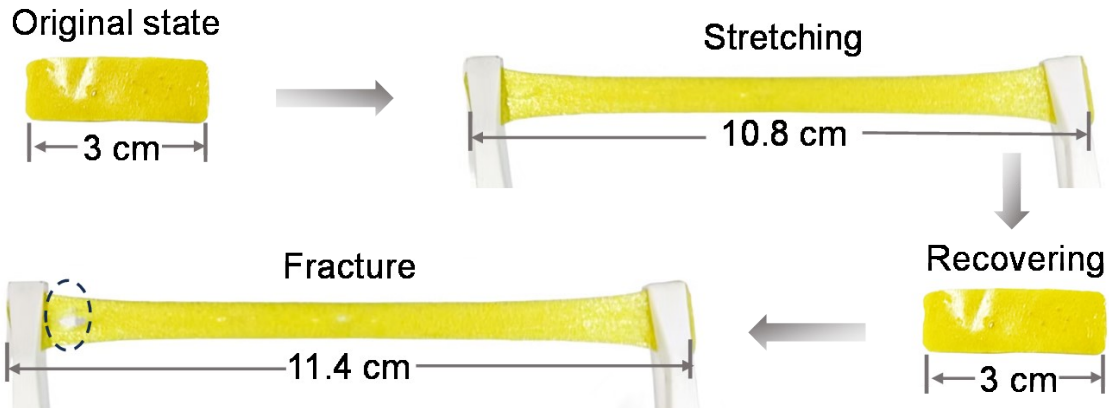


**Figure S5.** Stretchable image of G-0.1 M $FeCN^{4-/3-}$.

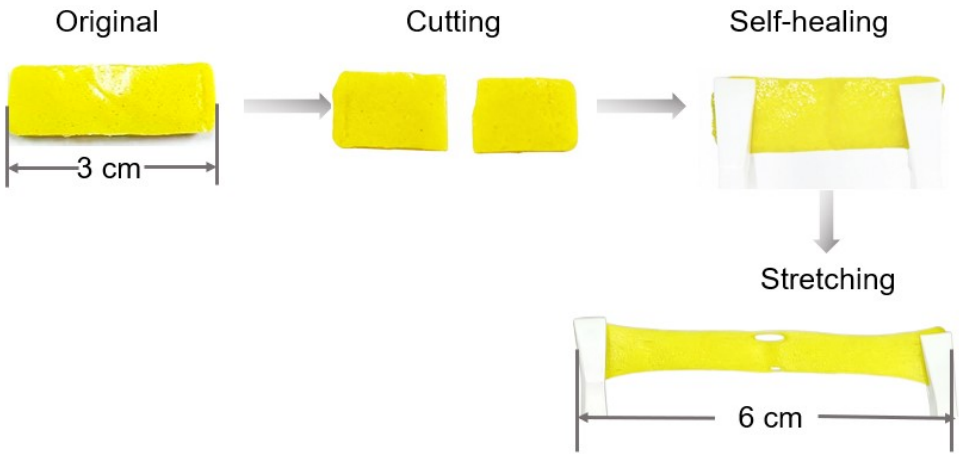


**Figure S6.** Image of self-healing for G-0.1M $FeCN^{4-/3-}$.

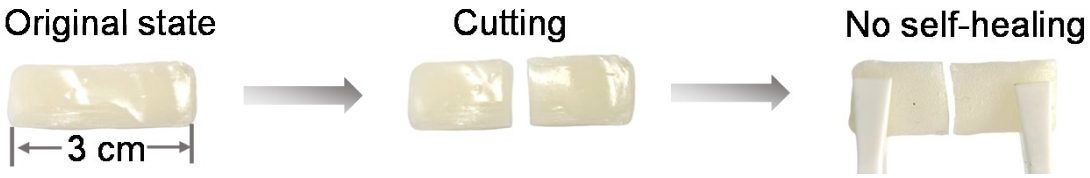


**Figure S7.** Image of no self-healing for pure gelatin.

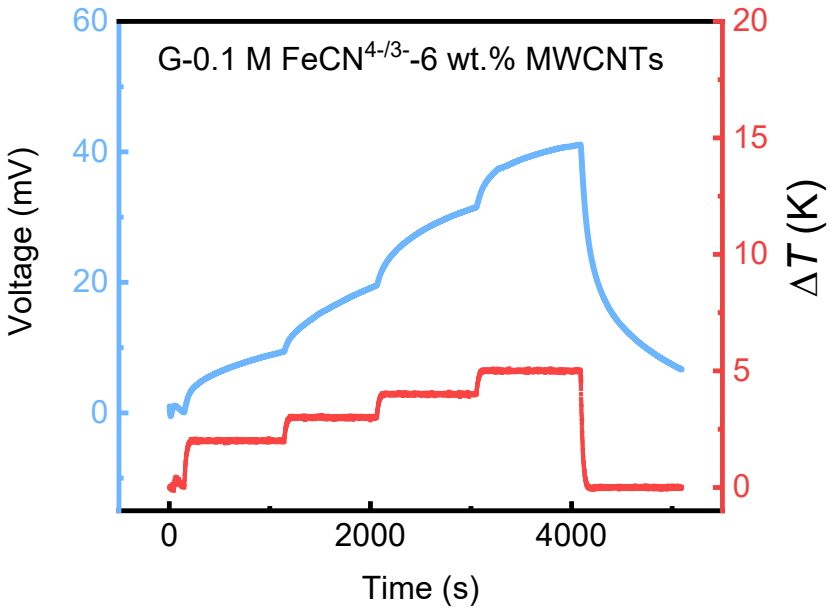


**Figure S8**. Voltage and temperature difference with dependence of time at $T_C$ = 313 K for G-0.1 M $FeCN^{4-/3-}$-6 wt.% MWCNTs.

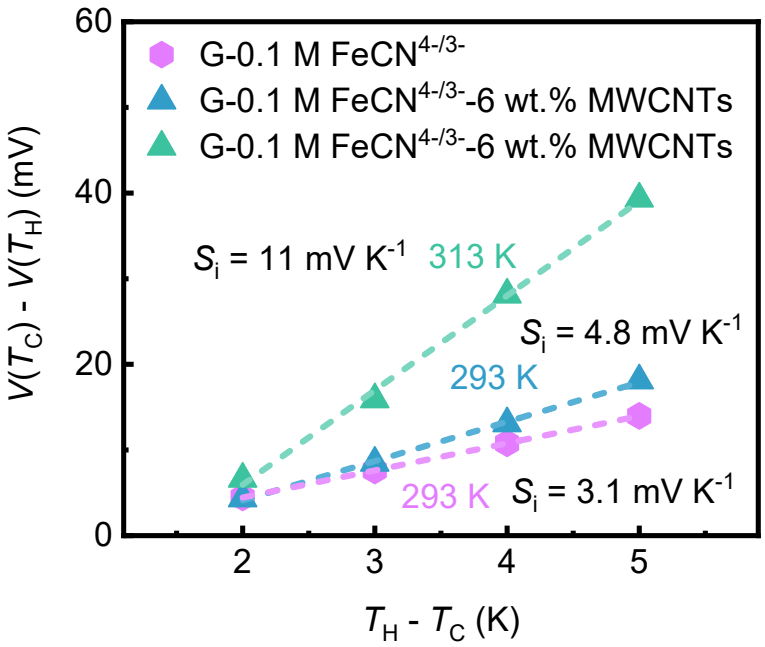


**Figure S9**. $V(T_C)$ - $V(T_H)$ with dependence of $T_H$ - $T_C$ for G-0.1 M $FeCN^{4-/3-}$ and G-0.1 M $FeCN^{4-/3-}$-6 wt.% MWCNTs at 293 and 313 K.

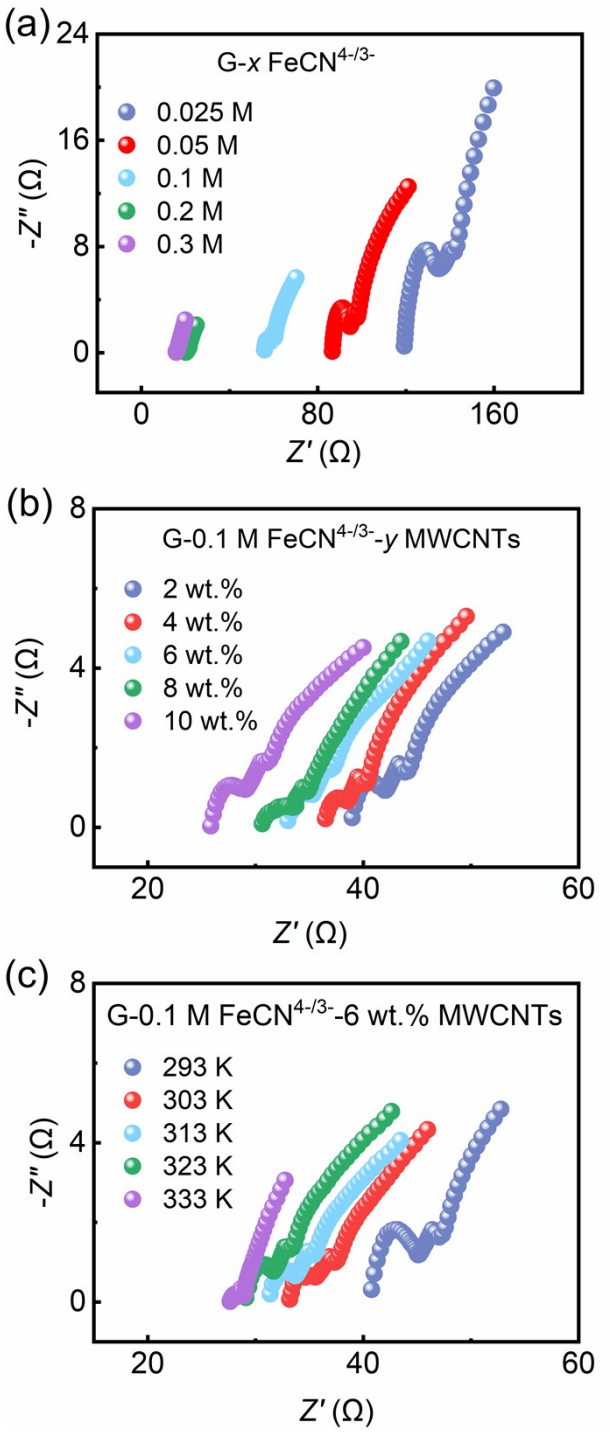


**Figure S10.** Electrochemical impedance spectroscopy (EIS) of i-TE gels (a) G-*x* $FeCN^{4-/3-}$ for *x* = 0.025, 0.05, 0.1, 0.2, and 0.3 M, (b) G-0.1 M $FeCN^{4-/3-}$-*y* MWCNTs for *y* = 2 wt.%, 4 wt.%, 6 wt.%, 8 wt.%, and 10 wt.%, (c) G-0.1 M $FeCN^{4-/3-}$-6 wt.% MWCNTs at *T* = 293, 303, 313, 323, and 333 K. Graphite paper was used as the electrode.

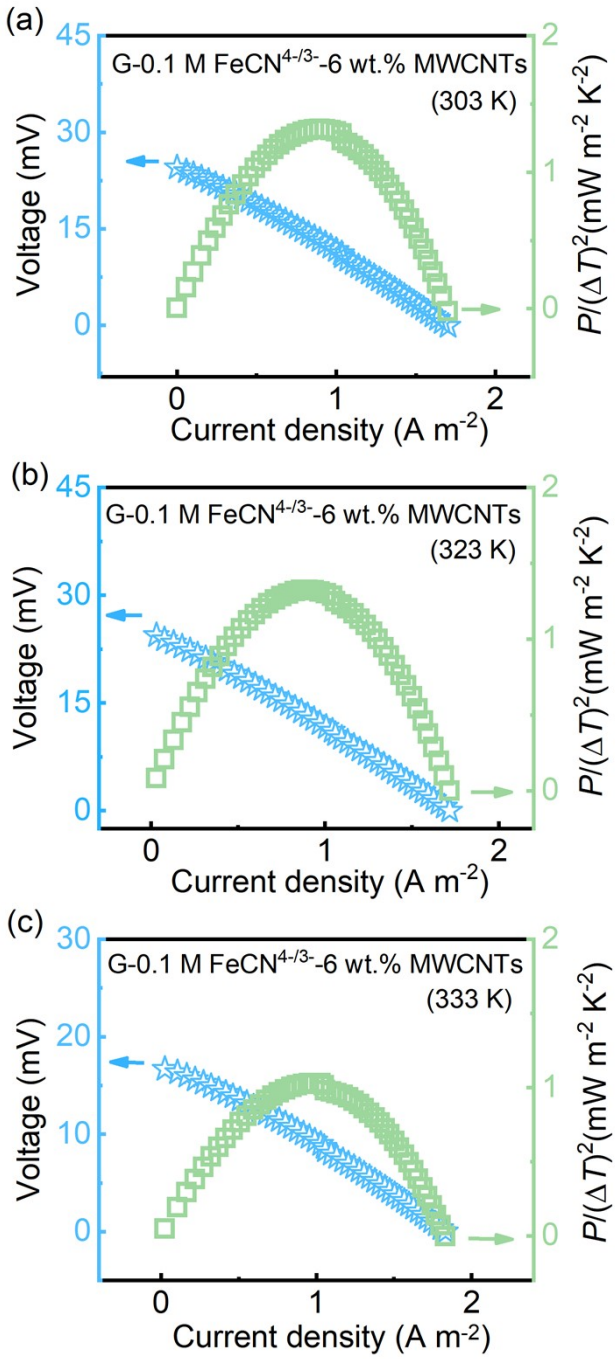


**Figure S11.** Voltage and $P/(\Delta T)^2$ with dependence of current density for i-TE gels G-0.1 M $FeCN^{4-/3-}$-6 wt.% MWCNTs at (a) $T$ = 303 K, (b) $T$ = 323 K, and (c) $T$ = 333 K.

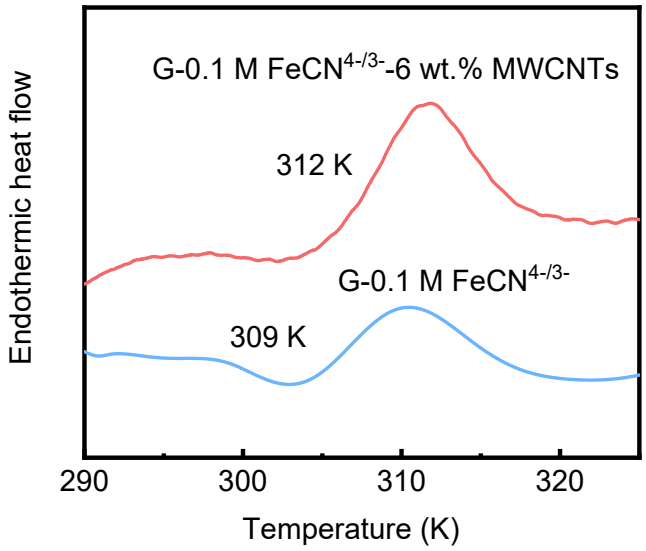


**Figure S12.** Differential scanning calorimetry (DSC) curves of G-0.1 M $FeCN^{4-/3-}$ and G-0.1 M $FeCN^{4-/3-}$-6 wt.% MWCNTs.

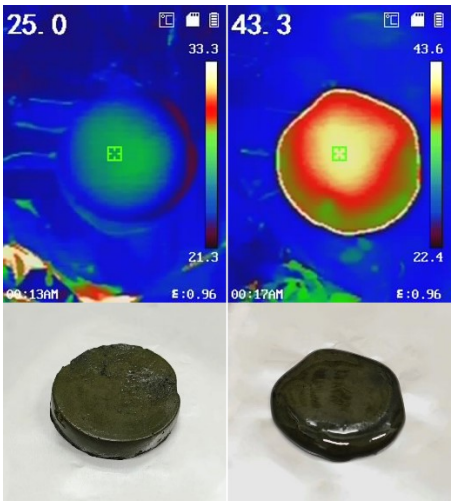


**Figure S13.** Infrared image of G-0.1 M $FeCN^{4-/3-}$-6 wt.% MWCNTs at 298 and 316.3 K on a hot plate.

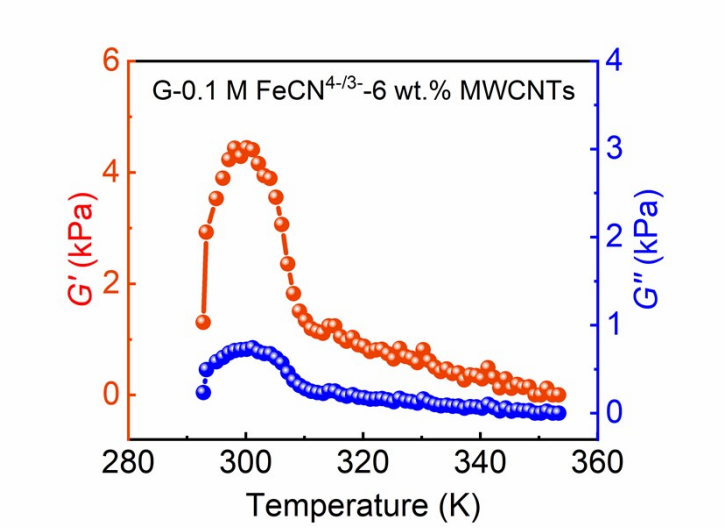


**Figure S14.** Temperature dependent storage modulus ($G'$) and loss modulus ($G''$) for the i-TE gel G-0.1 M $FeCN^{4-/3-}$-6 wt.% MWCNTs measured at $\omega$ = 1 Hz and $\gamma$ = 1%.

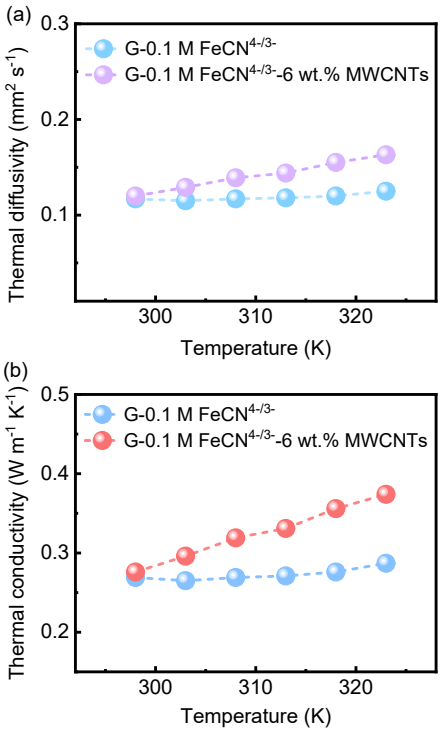


**Figure S15.** (a) Thermal diffusivity and (b) thermal conductivity for i-TE gels G-0.1 M $FeCN^{4-/3-}$ and G-0.1 M $FeCN^{4-/3-}$-6 wt.% MWCNTs.

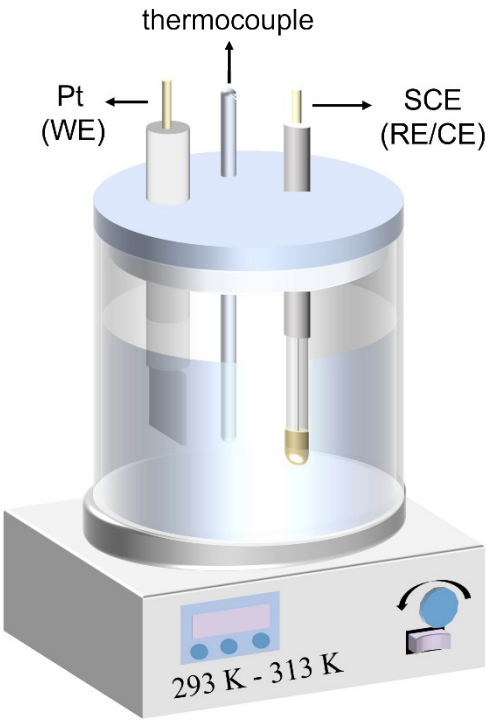


**Figure S16.** Isothermal three-electrode system for G-0.1 M $FeCN^{4-/3-}$-*y* MWCNTs (*y* = 0 wt.%, 2 wt.%, 4 wt.%, and 6 wt.%). Platinum was used as the working electrode (WE) and the saturated calomel electrode (SCE) was served as the reference electrode (RE) and counter electrode (CE).

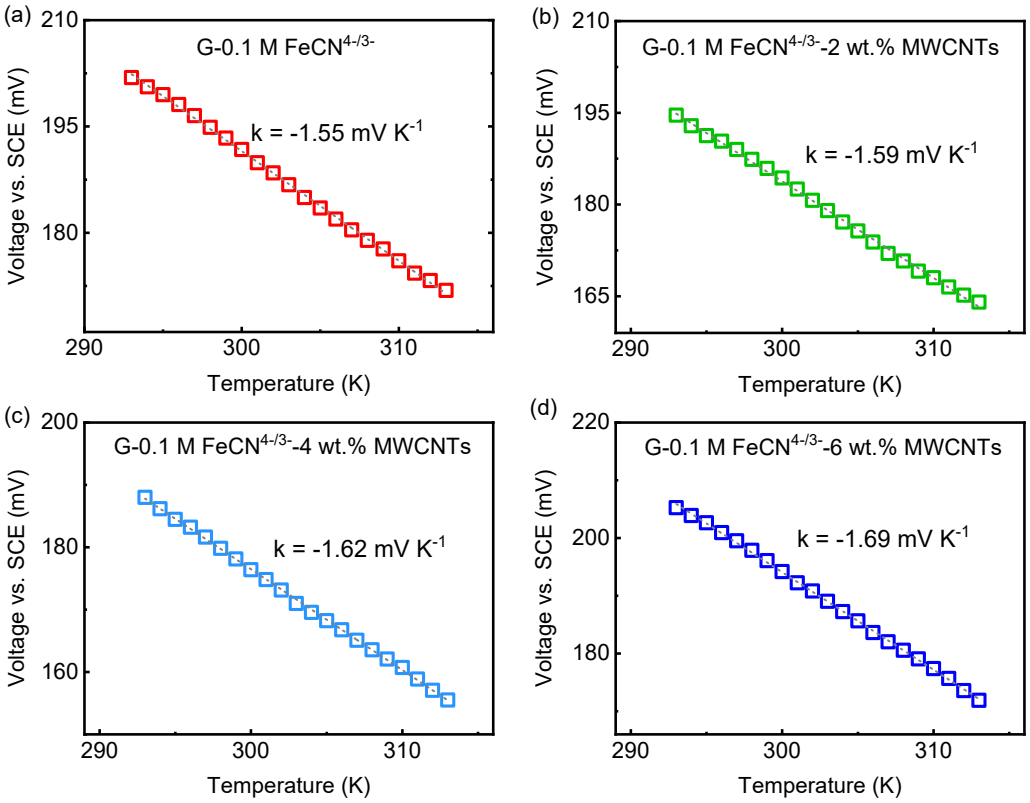


**Figure S17.** $V_{oc}$ vs. SCE with dependence of temperature ($T$ = 293-313 K) for G-0.1 M $FeCN^{4-/3-}$-$y$ MWCNTs with (a) $y$ = 0 wt.%, (b) $y$ = 2 wt.%, (c) $y$ = 4 wt.%, (d) $y$ = 6 wt.%.

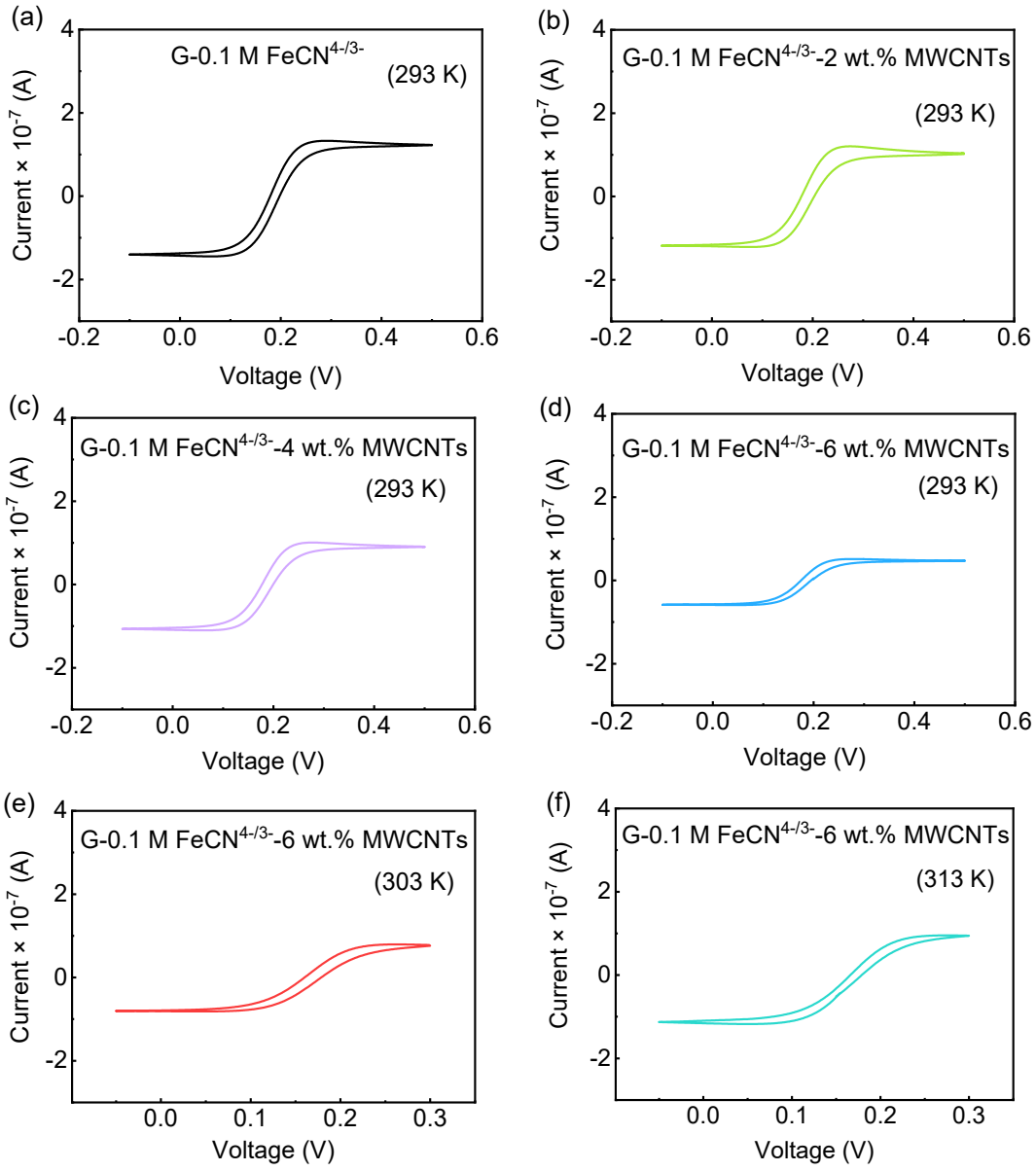


**Figure S18.** Cyclic voltammetry (CV) curves of (a) G-0.1 M $FeCN^{4-/3-}$ (293K), (b) G-0.1 M $FeCN^{4-/3-}$-2 wt.% MWCNTs (293 K), (c) G-0.1 M $FeCN^{4-/3-}$-4 wt.% MWCNTs (293 K), (d) G-0.1 M $FeCN^{4-/3-}$-6 wt.% MWCNTs (293K), (e) G-0.1 M $FeCN^{4-/3-}$-6 wt.% MWCNTs (303 K), (f) G-0.1 M $FeCN^{4-/3-}$-6 wt.% MWCNTs (313 K). The three-electrode system was employed. The Pt ultramicroelectrode (diameter: $d$ = 20 μm), Pt wire ($d$ = 0.5 mm), and SCE (saturated calomel electrode) were used as the working electrode, counter electrode, and reference electrode, respectively. CV curves were scanned from -0.1 to 0.5 V for (a-d) and from -0.05 to 0.3 V (e-f). Scan rate: 0.2 mV $s^{-1}$.

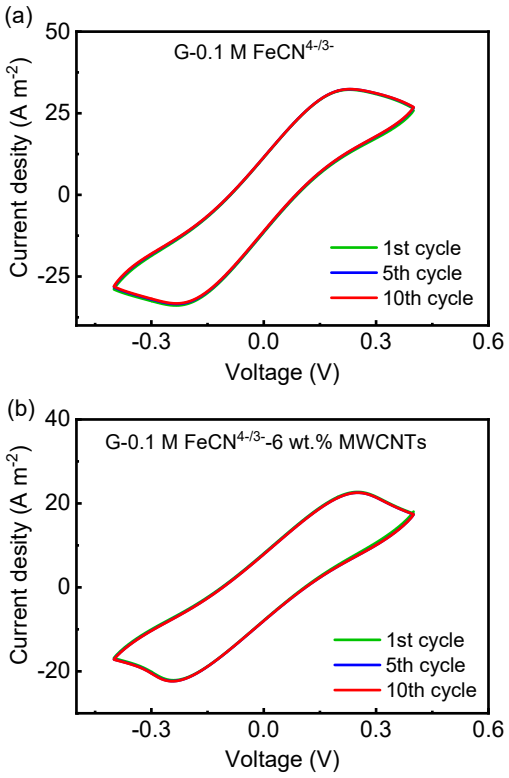


**Figure S19.** Cyclic voltammetry (CV) of G-0.1 M $FeCN^{4-/3-}$-*y* MWCNTs (a) *y* = 0 wt.%, (b) *y* = 6 wt.%. The scan rate was 10 mV $s^{-1}$. Pt was employed as the electrode.

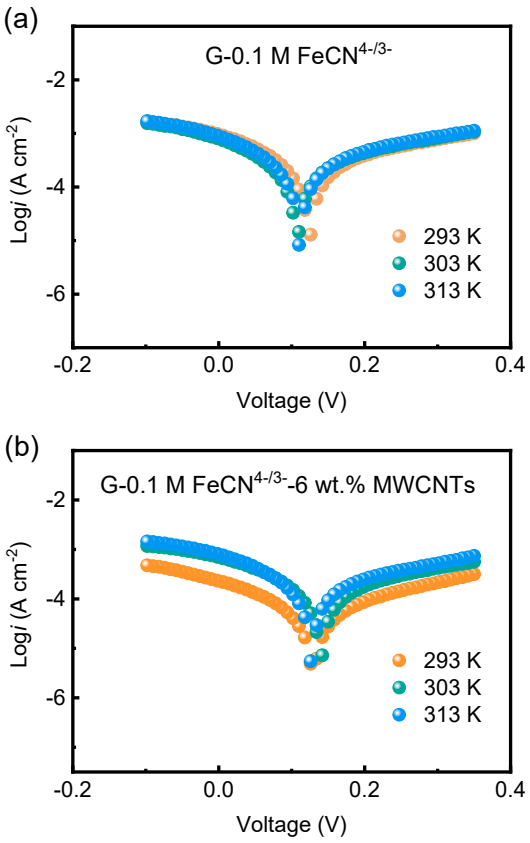


**Figure S20.** Tafel curves of i-TE gels (a) G-0.1 M $FeCN^{4-/3-}$ and (b) G-0.1 M $FeCN^{4-/3-}$-6 wt.% MWCNTs at $T$ = 293, 303, and 313 K. Electrode: graphite paper.

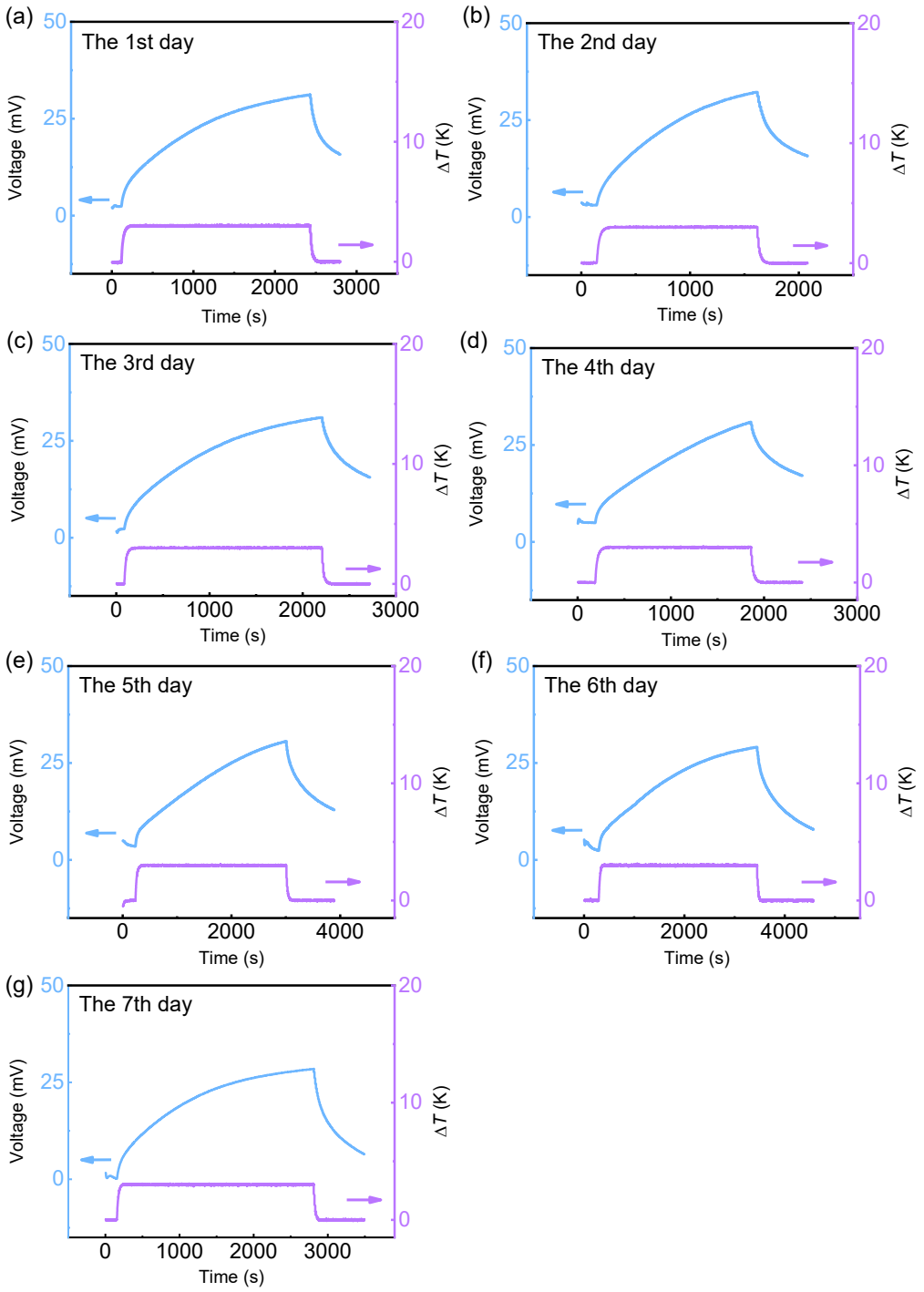


**Figure S21.** Voltage vs. time in 7 days measurement at $\Delta T = 3$ K for G-0.1 M $FeCN^{4-/3-}$-6 wt.% MWCNTs. (a) The 1st day, (b) The 2nd day, (c) The 3rd day, (d) The 4th day, (e) The 5th day, (f) The 6th day, (g) The 7th day. Humidity: 50%, oxygen content: 21%.

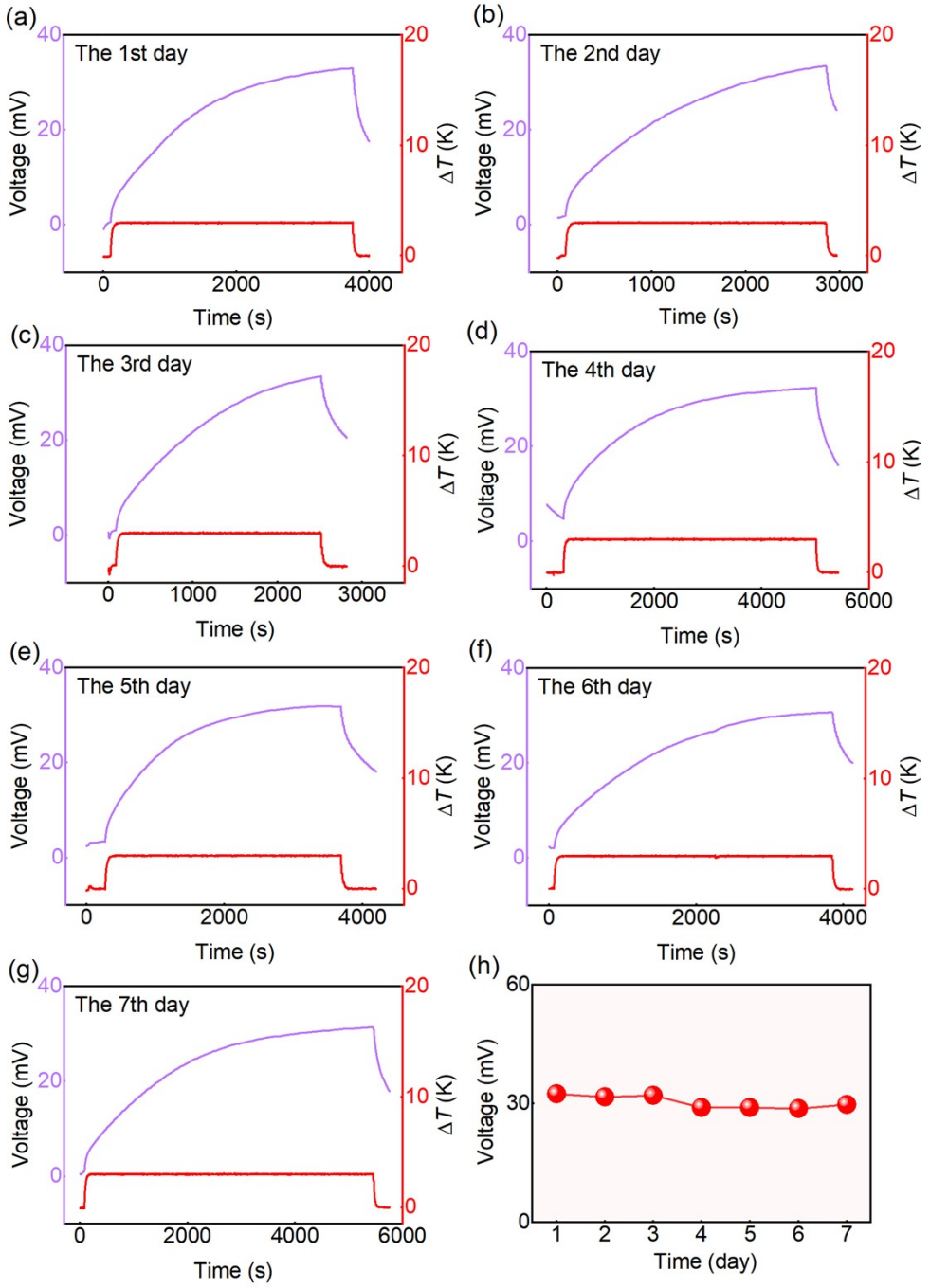


**Figure S22.** Voltage vs. time in 7 days measurement at $\Delta T$ = 3 K for G-0.1 M $FeCN^{4-/3-}$-6 wt.% MWCNTs. (a) The 1st day, (b) The 2nd day, (c) The 3rd day, (d) The 4th day, (e) The 5th day, (f) The 6th day, (g) The 7th day. Humidity: 90%, oxygen content: 21%.

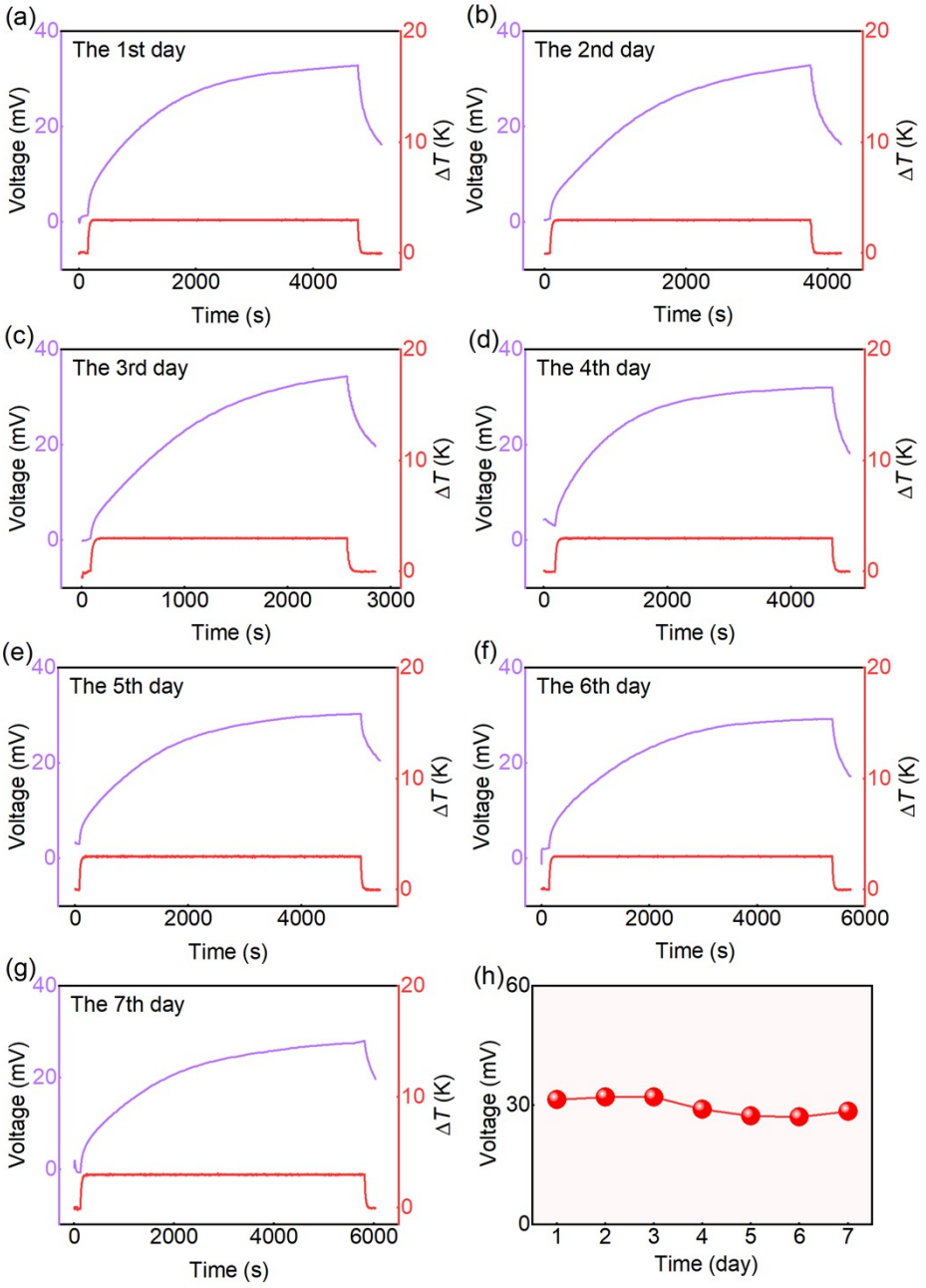


**Figure S23.** Voltage vs. time in 7 days measurement at $\Delta T = 3$ K for G-0.1 M $FeCN^{4-/3-}$-6 wt.% MWCNTs. (a) The 1st day, (b) The 2nd day, (c) The 3rd day, (d) The 4th day, (e) The 5th day, (f) The 6th day, (g) The 7th day. Oxygen content: 100%, humidity: 50%.

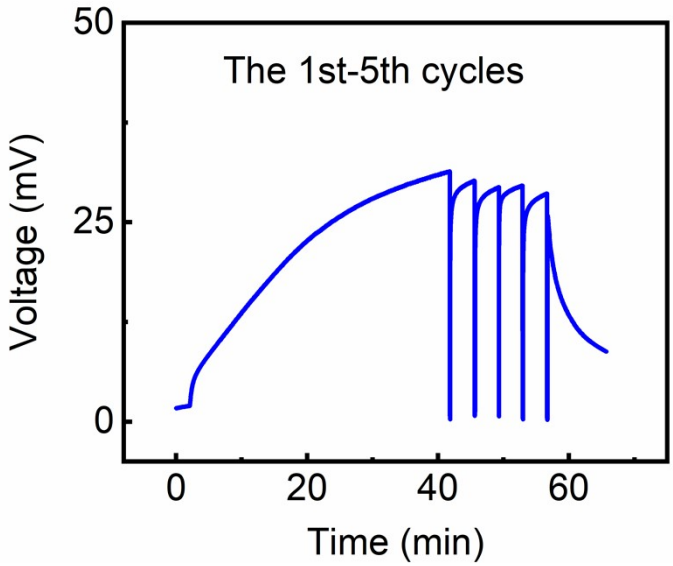


**Figure S24.** Voltage changes for initial 5 cycles at 313 K and $\Delta T$ = 3 K for the quasi-continuous discharge process.

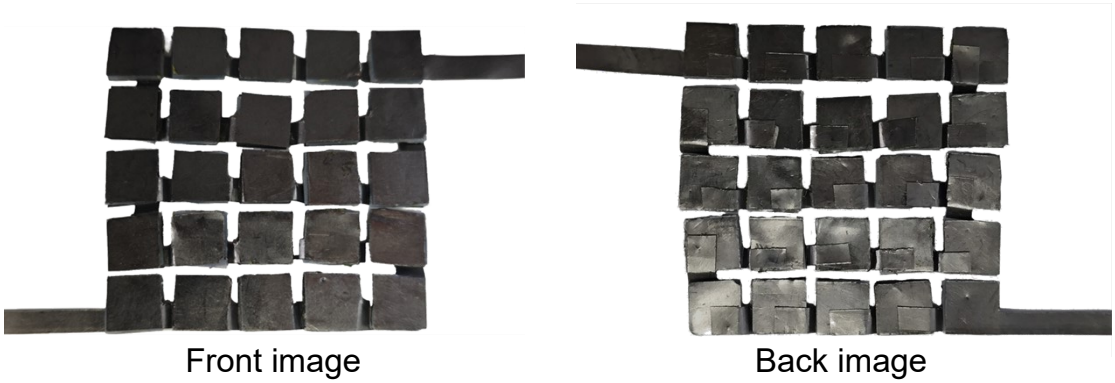


**Figure S25.** Image of i-TE gel device connected by 25 gel thermocells in series.

**Supporting Tables**

**Table S1.** Comprehensive comparison of $P_{max}/(\Delta T)^2$ (mW $m^{-2}$ $K^{-2}$), $S_i$ (mV $K^{-1}$), working temperature (K), self-healing, and stretchability for i-TE gels in this work and the reported results.

| Gels | $\lvert S_i \rvert$ | $P_{max}/(\Delta T)^2$ | Working temperature | Stretchability (%) | Self-healing | Ref. |
|---|---|---|---|---|---|---|
| Gelatin- $FeCN^{4-/3-}$ | 11 | 1.70 | 313 | 350 | Yes | This work |
| P(AM-co-AMPS) -$FeCN^{4-/3-}$ | 1.6 | 0.61 | 293 | 217 | Yes | 6 |
| PAM-$Fe^{2+/3+}$-DMAEA-Q | 2.0 | 0.10 | 223 | 250 | No | 7 |
| PVA-$Fe^{2+/3+}$ | 0.9 | 0.17 | 308 | 130 | No | 8 |
| Gelatin-$FeCN^{4-/3-}$ | 2.2 | 0.48 | — | 247 | No | 9 |
| BC-$FeCN^{4-/3-}$ | 2.3 | 0.07 | 304 | 167 | Yes | 10 |
| PVA/LaGG-$FeCN^{4-/3-}$ | 2.0 | 0.03 | 298 | 251 | Yes | 11 |

**Table S2.** Comparison of $P_{max}/(\Delta T)^2$ and voltage for i-TE gel device in this work and reported results.

| Gels | Voltage (V) | $P_{max}/(\Delta T)^2$ (mW m$^{-2}$ K$^{-2}$) | Cell number | Ref. |
|---|---|---|---|---|
| G-$FeCN^{4-/3-}$-MWCNTs | 0.105 | 0.8 | 4 | This work |
| PPF- $FeCN^{4-/3-}$ | 0.7 | 0.02 | 2 | 12 |
| BC-$FeCN^{4-/3-}$ | 0.82 | 0.02 | 6 | 13 |
| PMAA/PDMAPS-$I^-$/I- 3 | 1.8 | 0.07 | 20 | 14 |
| PNIPAM-$I^-$/I- 3 | 1 | 0.07 | 100 | 15 |
| Gelatin-KCl-$FeCN^{4-/3-}$ | 2.2 | 0.08 | 25 | 3 |
| CMC-$FeCN^{4-/3-}$ | 0.36 | 0.11 | 36 | 8 |
| PVA-$FeCN^{4-/3-}$ | 0.342 | 0.51 | 27 | 16 |

## Supporting references


1. M. J. Martín-Alfonso, F. J. Martínez-Boza and P. F. Luckham, *ACS Appl. Polym. Mater.*, 2025, **7**, 15896-15905.
2. P. R. Avallone, N. Russo, N. Gargiulo, N. Grizzuti and S. Costanzo, *Biomacromolecules*, 2025, **26**, 5450-5460.
3. C.-G. Han, X. Qian, Q. Li, B. Deng, Y. Zhu, Z. Han, W. Zhang, W. Wang, S.-P. Feng, G. Chen and W. Liu, *Science*, 2020, **368**, 1091-1098.
4. L. Yang, J. Chen, W. He, G. Li, C. Xie, W. Wang, D. Han, C.-G. Han and L. Niu, *Angew. Chem. Int. Ed*., 2025, **64**, e202511293.
5. A. J. Bard, L. R. Faulkner and H. S. White, *Anti-Corros. Methods Mater*., 2003, **50**.
6. Z. Lei, W. Gao and P. Wu, *Joule*, 2021, **5**, 2211-2222.
7. W. Gao, Z. Lei, C. Zhang, X. Liu and Y. Chen, *Adv. Funct. Mater*., 2021, **31**, 2104071.
8. Y. Liu, S. Zhang, Y. Zhou, M. A. Buckingham, L. Aldous, P. C. Sherrell, G. G. Wallace, G. Ryder, S. Faisal, D. L. Officer, S. Beirne and J. Chen, *Adv. Energy Mater*., 2020, **10**, 2002539.
9. X. Lu, Z. Mo, Z. Liu, Y. Hu, C. Du, L. Liang, Z. Liu and G. Chen, *Angew. Chem. Int. Ed*., 2024, **63**, e202405357.
10. J. Li, S. Chen, Z. Han, X. Qu, M. Jin, L. Deng, Q. Liang, Y. Jia and H. Wang, *Adv. Funct. Mater*., 2023, **33**, 2306509.
11. C. Tian, S. A. Khan, Z. Zhang, X. Cui and H. Zhang, *ACS Sens*., 2024, **9**, 840-848.
12. P. Yang, K. Liu, Q. Chen, X. Mo, Y. Zhou, S. Li, G. Feng and J. Zhou, *Angew. Chem. Int.*, 2016, **55**, 12050-12053.
13. Y. Zong, H. Li, X. Li, J. Lou, Q. Ding, Z. Liu, Y. Jiang and W. Han, *Chem. Eng. J*., 2022, **433**, 134550.
14. J. Shen, X. Huang, Y. Dai, X. Zhang and F. Xia, *Nat. Commun*., 2024, **15**, 9305.
15. J. Duan, B. Yu, K. Liu, J. Li, P. Yang, W. Xie, G. Xue, R. Liu, H. Wang and J. Zhou, *Nano Energy*, 2019, **57**, 473-479.
16. W. Gao, Z. Lei, W. Chen and Y. Chen, *ACS Nano*, 2022, **16**, 8347-8357.